

Observation of Quadratic (Charge-2) Weyl Point Splitting in Near-Infrared Photonic Crystals

Christina Jörg,* Sachin Vaidya, Jiho Noh, Alexander Cerjan, Shyam Augustine, Georg von Freymann,* and Mikael C. Rechtsman

Weyl points are point degeneracies that occur in momentum space of 3D periodic materials and are associated with a quantized topological charge. Here, the splitting of a quadratic (charge-2) Weyl point into two linear (charge-1) Weyl points in a 3D micro-printed photonic crystal is observed experimentally via Fourier-transform infrared spectroscopy. Using a theoretical analysis rooted in symmetry arguments, it is shown that this splitting occurs along high-symmetry directions in the Brillouin zone. This micro-scale observation and control of Weyl points is important for realizing robust topological devices in the near-infrared.

1. Introduction

Weyl materials have drawn significant interest over the last decade for their ability to support Weyl points (WPs), which are topologically protected degeneracies in 3D periodic systems. They have been examined in a wide range of physical systems such as conventional solids,^[1–7] photonic systems,^[8–18] acoustic systems,^[19–22] cold atoms,^[23,24] electric circuits,^[25] and

coupled resonator arrays.^[26,27] In photonics, WPs are sought for a range of applications such as designing large-volume single-mode lasers^[28] and mediating long-range interactions between quantum emitters,^[29,30] and as such they have been realized in a variety of optical and photonic systems^[8–18] spanning orders of magnitude in wavelength. WPs are quantized sources and sinks of Berry curvature in momentum space, analogous to magnetic monopoles. Therefore, they can be topologically characterized by the closed surface integral of the Berry

curvature; this “charge” is always an integer and is identical to the first Chern number. On the 2D surfaces of a Weyl material, this topological charge manifests through the appearance of surface-localized conduction channels, so-called Fermi-arc surface states, that connect two WPs with opposite charges. Since the Berry curvature vanishes identically in the Brillouin zone for structures with both spatial inversion and time reversal symmetry, it is necessary to break one or both of these symmetries to obtain WPs.

A Weyl point can possess an arbitrary integer charge, m , and can be described by the generic 3D Hamiltonian of the form,^[31]

$$\mathcal{H}(\mathbf{k}) = k_+^{|m|} \sigma_+ + k_-^{|m|} \sigma_- + k_z \sigma_z + \omega_0 I \quad (1)$$

where $k_{\pm} = (k_x \pm ik_y)$, $\sigma_{\pm} = 1/2(\sigma_x \pm i\sigma_y)$, $\sigma_{x,y,z}$ are the Pauli matrices, I is the identity matrix, and ω_0 is the frequency at which the WP occurs in the spectrum. The eigenvalues of $\mathcal{H}(\mathbf{k})$ describe the two bands in the vicinity of the WP and are given by

$$\lambda_{\pm} = \omega_0 \pm \sqrt{(k_x^2 + k_y^2)^{|m|} + k_z^2} \quad (2)$$

From Equation (2) it is evident that the leading order $k_{x,y}$ -dependence in the dispersion around a WP is governed by its charge and henceforth, charge-1 WPs will be referred to as “linear” and charge-2 WPs as “quadratic.”

While linear WPs have been extensively studied, higher-charged WPs have received relatively less attention. These exotic WPs, sometimes referred to as unconventional WPs, have markedly different properties than their conventional counterparts such as higher-order algebraic dispersion, multiple Fermi-arc surface states and large density of states for high charge ($m \geq 2$). Higher-charged WPs are known to occur in nonsymorphic crystals due to the stabilization of multiple linear WPs at high symmetry points in momentum space.^[12,32,33] In photonics, quadratic WPs were predicted^[14] and observed in all-dielectric


C. Jörg, S. Vaidya, J. Noh, A. Cerjan, M. C. Rechtsman
Department of Physics
The Pennsylvania State University
University Park, PA 16802, USA
E-mail: czj5278@psu.edu

C. Jörg, S. Augustine, G. von Freymann
Physics Department and Research Center OPTIMAS
Technische Universität Kaiserslautern
Kaiserslautern 67663, Germany
E-mail: georg.frey mann@physik.uni-kl.de

J. Noh
Department of Mechanical Science and Engineering
University of Illinois at Urbana-Champaign
Urbana, IL 61801, USA

A. Cerjan
Center for Integrated Nanotechnologies
Sandia National Laboratories
Albuquerque, NM 87123, USA

G. von Freymann
Fraunhofer Institute for Industrial Mathematics ITWM
Kaiserslautern 67663, Germany

 The ORCID identification number(s) for the author(s) of this article can be found under <https://doi.org/10.1002/lpor.202100452>

© 2021 The Authors. Laser & Photonics Reviews published by Wiley-VCH GmbH. This is an open access article under the terms of the Creative Commons Attribution License, which permits use, distribution and reproduction in any medium, provided the original work is properly cited.

DOI: 10.1002/lpor.202100452

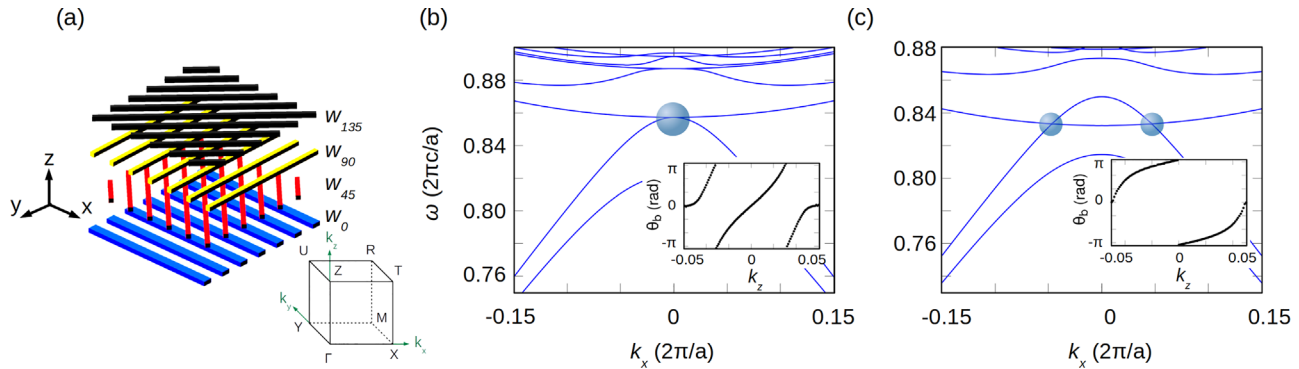


Figure 1. a) An exploded view of the chiral woodpile PhC (one unit cell in z) and its Brillouin zone. Each layer of rods has a 50% overlap in z with neighboring layers. b) Band structure of the chiral woodpile PhC, made out of dielectric rods ($\epsilon = 2.31$), with equal widths $w = 0.09a$ for all rods at $k_y = k_z = 0$ showing bands 3 to 8. The quadratic WP at Γ is marked with a blue circle. The inset shows a plot of the Berry phase for band 4 around Γ . The double winding indicates that the degeneracy has a charge of 2. c) The band structure of the same chiral woodpile PhC as in (b) but with increased rod width w_0 in each unit cell. The linear WPs that occur due to the splitting of the quadratic WP in (b) are marked with blue circles. The inset shows a plot of the Berry phase for band 4 around one of the degeneracies. The single winding indicates that the degeneracy has a charge of 1.

woodpile-like structures.^[16] Such structures exhibit several additional symmetries and therefore provide an ideal platform for tuning the locations of linear WPs that can form from splitting a quadratic WP due to symmetry breaking.^[33,34] This tunability of WPs could be of importance in the realization of 3D large-volume, single-mode lasing devices that rely on the vanishing photonic density of states at frequency-isolated linear WPs.^[28]

In this article, we experimentally demonstrate that under careful symmetry breaking, quadratic WPs can be split into two linear WPs of the same charge. We show by analyzing the underlying symmetries of the structures that for certain choices of defects this splitting occurs strictly along high symmetry directions in momentum space. We also show that the momentum-space separation of the resulting linear WPs can be readily controlled via geometric parameters of the structure. While WPs have mostly been observed in large-scale structures with mm- or cm-scale lattice constants,^[9,10,35] our platform of choice is a micron-scale 3D photonic crystal (PhC) with low dielectric contrast which is fabricated by a two-photon polymerization process.^[36] This allows for the realization of WPs at near-infrared wavelengths that are characterized using Fourier transform infrared (FTIR) spectroscopy.

2. Simulations and Symmetry Analysis

The particular structure that we employ to realize this phenomenon is a chiral woodpile PhC whose unit cell consists of stacked and partially overlapping layers of rods that have a relative 45° in-plane rotation between them as shown in **Figure 1a**. The lattice constant in all three directions is $a = 2.1 \mu\text{m}$. The four rods in the unit cell have height h and widths $w_0, w_{45}, w_{90}, w_{135}$ where the subscripts identify the rods by their angle of orientation with respect to the x -axis. The rods are made out of a nearly lossless, nonmagnetic dielectric material of dielectric constant $\epsilon = 2.31$ (see Experimental Section). Due to the chirality of this structure, inversion symmetry is broken which allows WPs to exist. Furthermore, when all rod widths and heights are equal, this structure belongs to the nonsymmorphic space group $P4_222$ (# 93), which has a screw axis along the z direction. This screw symmetry, defined by a 90° rotation in the

x - y plane and $a/2$ shift along the z direction, results in the presence of a quadratic WP at the Brillouin zone center (Γ), as shown in **Figure 1b**, and corners (\mathbf{R}) (see Supplementary Material for dispersion).

Instead, when the rod width in one layer in the unit cell is taken to be different from the widths of the other three layers, the screw symmetry is broken, resulting in a splitting of the quadratic WP into two linear WPs as shown in **Figure 1c**. For example, when a width defect is introduced such that $w_{45} = w_{90} = w_{135} = w$ and $w_0 \neq w$, the space group of the structure is reduced to $P222$ (# 16). While this subgroup does not contain the screw symmetry, it retains C_2 rotations about the x , y , and z axes that restrict the splitting directions of the WPs to high symmetry lines in momentum space. This can be argued as follows: Let the splitting associated with this change in space group by a small perturbation result in two linear WPs, one of which is located at a generic momentum point (k_x, k_y, k_z) . The location of both WPs can be inferred from the symmetry operations of the space group $P222$ and time reversal symmetry as they must either map to themselves or to each other under these operations. Time reversal symmetry requires a WP to be located at $(-k_x, -k_y, -k_z)$. However, the aforementioned C_2 rotations require a WP to be located at $(-k_x, k_y, -k_z)$, $(k_x, -k_y, -k_z)$, and $(-k_x, -k_y, k_z)$. Since there are only two linear WPs that can occur from the splitting of a single quadratic WP, at least two components of these momentum vectors must be set to 0 or π/a such that they map to themselves under a sign flip. As a result, for the quadratic WP at Γ , the symmetry-consistent directions of splitting are $\Gamma - X$, $\Gamma - Y$, or $\Gamma - Z$, and for the quadratic WP at \mathbf{R} , the symmetry-consistent directions of splitting are $\mathbf{R} - \mathbf{U}$, $\mathbf{R} - \mathbf{T}$, or $\mathbf{R} - \mathbf{M}$. A similar analysis shows that the splitting can be made to occur along diagonal directions in momentum space (e.g., along $\Gamma - M$ for the WP at Γ) when w_{45} or w_{135} is chosen to be different from the other three rod widths. In the most general case where all four rod widths are different, the space group is further reduced to $P2$ (#3) which retains C_2 rotation about the z axis. This only restricts the splitting to occur in the $k_z = 0$ plane or along $\Gamma - Z$ for the quadratic WP at Γ and $k_z = \pi/a$ plane or along $\mathbf{R} - \mathbf{M}$ for the quadratic WP at \mathbf{R} . For the remainder of this article, we will focus on the case

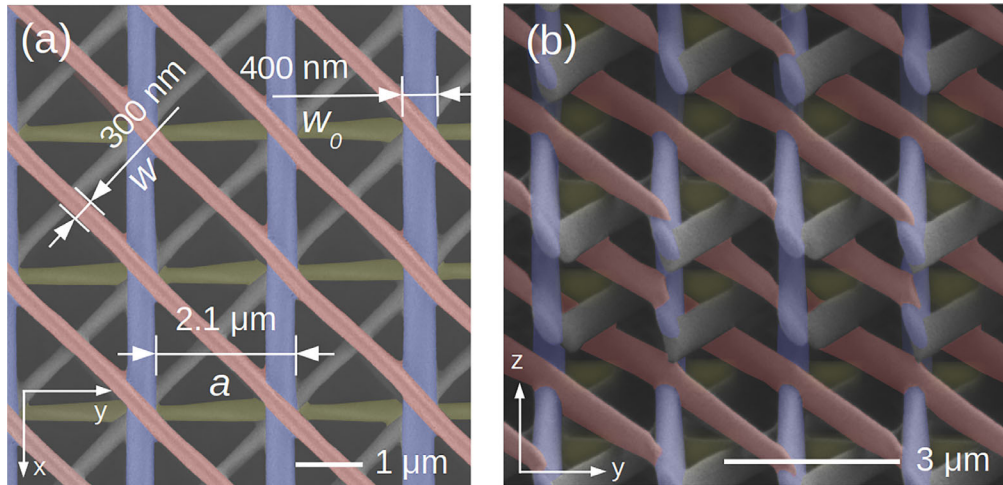


Figure 2. False color scanning electron microscope image of a typical chiral woodpile photonic crystal with increased rod width w_0 in the blue rods. a) Top view, b) tilted side view of the structure.

where a width defect is introduced in a single layer in each unit cell such that $w_{45} = w_{90} = w_{135} = w$ and $w_0 \neq w$.

To demonstrate the topological nature of WPs in the split and unsplit cases, we directly calculate their topological charges from the electromagnetic eigenmodes extracted from MIT Photonic Bands (MPB).^[37] Since WPs act as sources or sinks of Berry curvature, their charge can be obtained by integrating the Berry curvature over a closed sphere enclosing the WP in momentum space. Alternatively, this can also be calculated using a series of line integrals of Berry connection on closed contours that are sampled from such a sphere. These line integrals represent the geometric phase, called the Berry phase (θ_B), acquired by the eigenmodes as they are adiabatically transported around the closed contours. In the discrete form, θ_B on one such contour (C) is given by^[38]

$$\theta_B(C) = -\text{Im} \ln \left(\prod_{i=1}^N \frac{\langle \psi(\mathbf{k}_i) | \psi(\mathbf{k}_{i+1}) \rangle}{|\langle \psi(\mathbf{k}_i) | \psi(\mathbf{k}_{i+1}) \rangle|} \right) \quad (3)$$

where the index i discretizes the contour C into N points and $|\psi(\mathbf{k}_i)\rangle$ is the periodic part of the magnetic field eigenmode of the PhC at the momentum point \mathbf{k}_i . These contours can be chosen to lie parallel to the k_x - k_y plane and θ_B can therefore be plotted as a function of k_z . The topological charge of the WP is the winding number of $\theta_B(k_z)$. The plots for θ_B for the split and unsplit cases are shown in the insets of Figure 1b,c which confirm that the degeneracy at Γ is a quadratic WP of charge +2 and the split degeneracies along the Γ -X direction are linear WPs of charge +1 each.

3. Experimental Results

For the experiment, we fabricate chiral woodpile PhCs via two-photon lithography of a liquid negative-tone photoresist (IP-Dip, refractive index = 1.52) using a Nanoscribe professional GT. We print several samples of this PhC with a lattice constant of 2.1 μm with varying values of w_0 , while fixing w to 0.2 μm for the sym-

metry broken samples. Due to the voxel's height in z , adjacent layers overlap by $\approx 50\%$ of the rod height. A scanning electron microscope image of a typical sample is shown in **Figure 2**. For characterizing the fabricated PhC, we measure the angle-resolved transmittance via FTIR. Details about the fabrication and measurement setup can be found in the Experimental Section.

For the case of all equal rod widths, we observe a quadratic WP at 2.2 μm wavelength at the Γ point (**Figure 3a**). As previously described, an increase in w_0 splits the WP along the Γ -X direction into two linear WPs. This splitting can be seen as a spectral feature corresponding to the two involved bands piercing through each other with the linear WPs occurring at their intersection points as shown in Figure 3b-e. Furthermore, the angular separation between the two linear WPs increases with w_0 . Along the orthogonal direction, Γ -Y, the separation of the same spectral feature indicates that the two bands move apart and are nondegenerate (see Supporting Information). To compare our experimental results with theory, we also perform RCWA (rigorous coupled-wave analysis) simulations as implemented in Stanford Stratified Structure Solver (S^4).^[39] to obtain the transmission spectrum of this PhC. The simulated spectra are plotted in Figure 3f-j and show an excellent agreement with the experimentally obtained data. Moreover, the sharp spectral features match the $k_z = 0$ Weyl bands obtained from MPB (dashed lines in Figure 3f-j) allowing for a direct observation of the splitting.

We extract the angular separation θ between the two linear WPs from the experimental data and plot it as a function of the symmetry-breaking parameter $1 - w/w_0$ in **Figure 4**, demonstrating the tunable nature of WP splitting in this structure. In our experiment, the separation of WPs in momentum space is found to be a monotonic function of the symmetry-breaking parameter, however we note that this is not true in general. For higher dielectric contrast, the separation of the WPs can first increase and then decrease to zero for increasing values of the symmetry-breaking parameter. This can lead to the formation of accidental quadratic WPs which are not symmetry protected but are obtained on the fine tuning of parameters (see Supporting Information for an example).

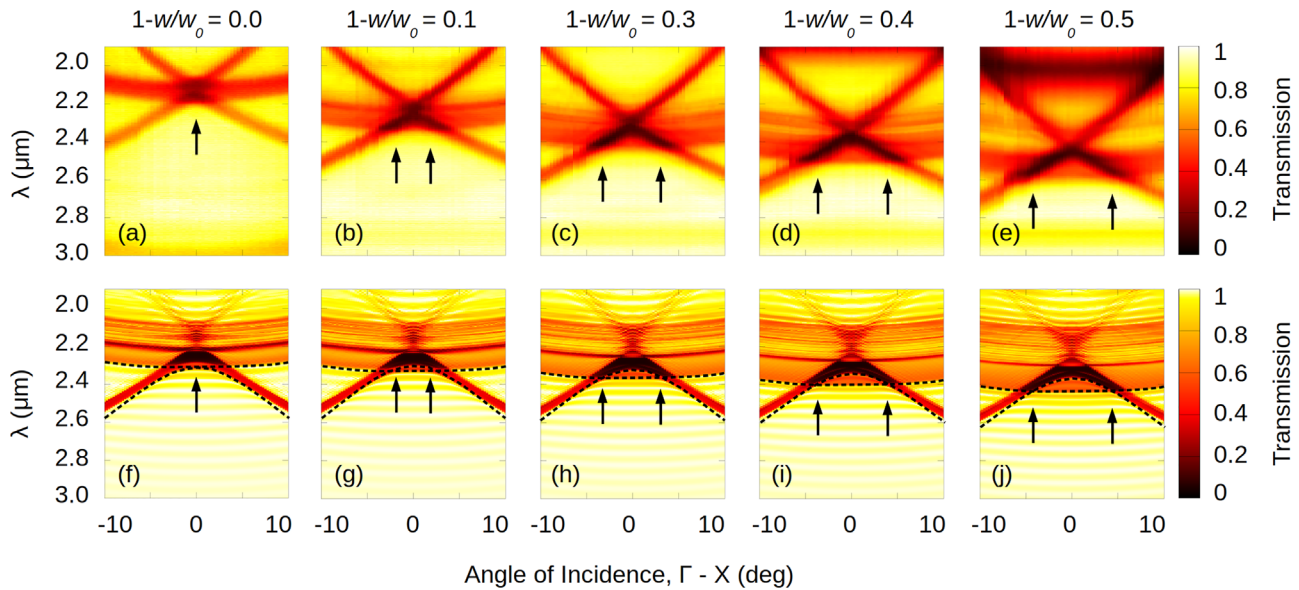


Figure 3. a–e) Measured angle-resolved FTIR spectra of the chiral woodpile PhC with varying values of the width w_0 . The locations of the WPs are marked with arrows. f–j) The corresponding RCWA simulated spectra of the chiral woodpile PhC. The dashed black lines are the $k_z = 0$ bulk bands calculated from MPB.

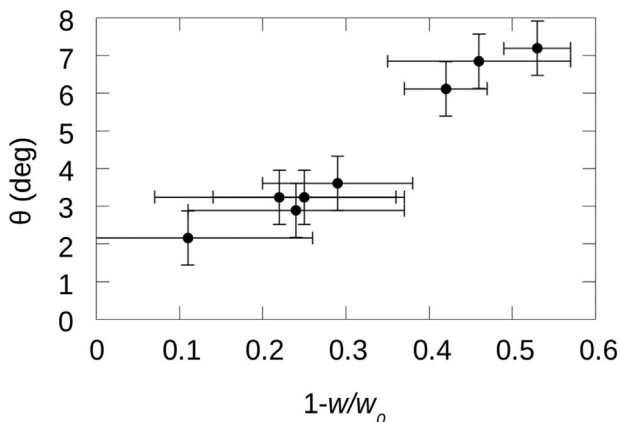


Figure 4. The angular separation of WPs, θ , as a function of the symmetry-breaking parameter, $1 - w/w_0$. All data points correspond to samples that were fabricated with the same value of w .

At low dielectric contrast, the WPs are embedded inside the k_z -projected bands of the PhC which could obscure the dispersion features of the WPs in the spectrum. However, we observe that the $k_z = 0$ Weyl bulk bands are clearly visible as boundaries of sharp features in the spectrum as indicated by the dashed lines in Figure 3f–j. To explain this observation, we perform a coupling analysis similar to refs. [16,40–43] which reveals that the relevant projected bands are nearly of either s- or p- character and hence couple selectively to light of these polarizations (see Supporting Information). This selective coupling results in the boundary of the projected bands, corresponding to $k_z = 0$ bulk bands, appearing as sharp drops in the transmission of polarized light allowing for the observation of WPs despite the lack of a local bandgap.

4. Bulk-Boundary Correspondence and Surface States

Perhaps the most direct physical manifestation of the nontrivial topology of a WP is the presence of surface states that form Fermi-arcs connecting WPs of opposite charges. Interestingly, this property is closely related to that of unidirectional edge states found in 2D Chern insulators. We now present a numerical exploration of the surface states associated with both the quadratic and linear WPs in our structure. Since the WPs of interest occur near the Brillouin zone center, the surface states lie above the light line of air. As a result, they are leaky resonances that radiate away from the surface with a finite lifetime. At low dielectric contrast such as in our experiment, the lifetime of such resonances can be so small that they are effectively unobservable in experiment and hard to extract and analyze numerically. To overcome this difficulty, we consider an interface between two chiral woodpile PhCs with opposite chirality for our analysis. This leads to a doubling of the number of surface states due to the presence of WPs on both sides of the interface. Moreover, the surface states originating from both structures are degenerate in frequency and momentum and can therefore hybridize to form states with even and odd symmetry with respect to the mirror plane at the interface. Nevertheless, the topological origin of these surface states can be directly confirmed by examining the surface spectrum along a circular contour that encloses the projection of the WPs.

We consider a system consisting of two chiral woodpile PhCs with opposite chirality and equal rod widths in all layers that meet at an interface parallel to the $y = 0$ plane. The surface band structure calculated along a circular loop in the k_x - k_z plane enclosing the quadratic WP at Γ is shown in Figure 5a. This loop has a radius of $0.05 (2\pi/a)$ and is parametrized by a single angular variable $0 \leq t/(2\pi) < 1$. The surface band structure reveals the existence of two pairs of hybridized states that cross the non-trivial

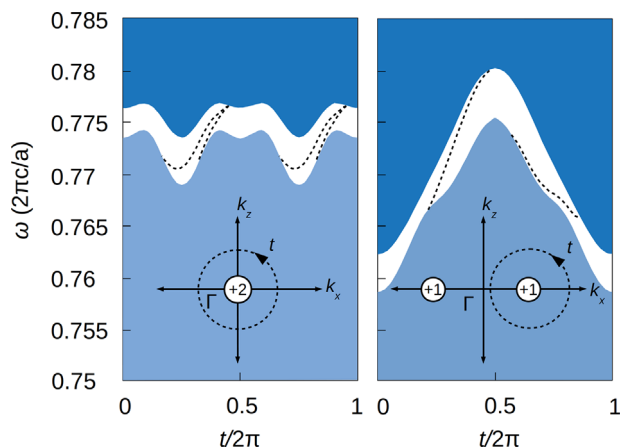


Figure 5. Surface states associated with the WPs at the interface between two low-contrast chiral woodpile PhCs with opposite chirality. a) The k_y -projected band structure along the circular loop, parameterized by t , enclosing the quadratic WP at Γ . The nontrivial gap formed along the loop contains two pairs of hybridized surface states (dashed lines) with even and odd symmetry with respect to the mirror plane at the interface. The blue solid colors are projections of the bulk bands. b) The k_y -projected band structure along the circular loop enclosing one of the split linear WPs, showing only a single pair of even and odd surface states. Note that slightly thicker rods ($w = 0.175a$) are used here compared to Figure 1 in order to open a band gap along the loops shown in the inset.

gap formed along the loop. Due to the bulk-boundary correspondence principle, the number of surface states implies that the magnitude of charge of the enclosed WPs is 2. Next, we consider the same simulation but for an increased rod width w_0 that splits the quadratic WP. The surface band structure along a loop of radius $0.033 (2\pi/a)$ enclosing just one of the linear WPs is shown in Figure 5b which reveals only one pair of surface states in the gap formed along the loop. This indicates that the charge of the enclosed WP has magnitude of 1.

5. Conclusion

In conclusion, we have observed the splitting of a quadratic Weyl point into two linear Weyl points in a low-contrast 3D PhC. We find that the splitting can be made to occur strictly along high-symmetry directions in momentum space, a consequence of controlled symmetry breaking and that their separation can be readily tuned via the geometric parameters of the crystal. The micron-scale periodicity of our structure allows us to access Weyl points in the near-infrared optical spectrum. Our approach opens new avenues for designing large-volume single-mode lasers^[28], using Weyl points and Fermi-arc surface states in microscale photonic structures, relevant to near-infrared optics.

6. Experimental Section

Fabrication: For the fabrication of the chiral photonic woodpile samples in the IP-Dip resist, a Nanoscribe Professional GT was used at a scan speed of 20 mm s^{-1} and laser power of 62%, which corresponded to 34 mW on the entrance lens of the objective. The structures were printed onto Menzel cover slips (borosilicate glass). Since the dip-in configuration of the Nanoscribe was used, the cover slips needed to be coated with

approximately 13 nm of Al_2O_3 in order to facilitate interface finding. The coated cover slips showed a transmission of greater than 75% for all wavelengths used in the measurements. After printing, the samples were developed for 10 min in PGMEA and 10 min in isopropanol, subsequently. They were then transferred to a solution of 150 mg Irgacure 651 in 24 mL of isopropanol and illuminated for 60 s with UV light from an Omnicure S2000 with 95% iris opening. This post-print UV curing^[44] was required to increase the stability of the woodpile structures. In the end, the samples were blow-dried in a stream of nitrogen. The complete footprint of a typical structure was approximately 1 mm^2 with 20 layers in height. To achieve such a large footprint within reasonable writing time elaborate stitching was used: The structures were printed in portions of 4×4 angled blocks between which the stage was moved for larger travel distance. Inside each block and layer the samples were printed using the galvanometer-scanning in combination with piezo-stitching for reduced vignetting and more precise positioning. The alignment of the stage, piezo, and galvo axes was ensured by employing the axis transformation implemented in NanoWrite. The structural parameters were determined via scanning electron microscopy and are listed in Supporting Information. While the usual rods consisted of just one printed line, the defect rod width was increased by printing multiple lines at a hatching distance between 10 and 50 nm. For the structure in Figure 3b the laser power used for printing the w_0 -rods was decreased to 55%.

Measurement: For the measurement of the spectra of the woodpile samples, the Hyperion 3000 microscope attached to a Bruker Vertex v70 FTIR was used. The spectra were taken in transmission mode with a halogen lamp and a MCT detector cooled by liquid nitrogen. To increase k -space resolution the lower $15\times$ Cassegrain objective was covered except for a pinhole of 1 mm in diameter, such that a nearly collimated beam was obtained. The spread of this beam was estimated to be approximately $\pm 0.3^\circ$ in the direction along which we measure (the k_x direction (in Figure 3)), and $\approx \pm 2^\circ$ perpendicular to that.^[45] The sample was then tilted with respect to the beam along its x -axis, around perpendicular incidence of the beam. This was done by tilting the sample holder in steps of $\approx 0.4^\circ$. As the position of perfect perpendicular incidence from the sample positioning cannot be determined (within an error of approximately 5°), spectra for both positive and negative tilting angles were taken, and the Γ point was determined from the symmetry of the measured angle resolved transmittance spectra. All spectra were referenced to the transmission of the blank substrates, and individually scaled to their maximum at each angle. For each angle we averaged over 64 measurements with an FTIR resolution set to 4 cm^{-1} in wavelength. The small dip in transmittance around $2.8 \mu\text{m}$ wavelength, constant across angles, was due to the absorption in the IP-Dip^[46]. The spectra were post-processed to remove fringes that appeared in the spectra due to multiple reflections in the glass and Al_2O_3 .

Supporting Information

Supporting Information is available from the Wiley Online Library or from the author.

Acknowledgements

C.J. and S.V. contributed equally to this work. C.J. gratefully acknowledges funding from the Alexander von Humboldt Foundation within the Feodor-Lynen Fellowship program. G.v.F. acknowledges funding by the Deutsche Forschungsgemeinschaft through CRC/Transregio 185 OSCAR (project No. 277625399). The authors would like thank the Nano Structuring Center Kaiserslautern for technical support. M.C.R., S.V., J.N., and A.C. acknowledge the support of the U.S. Office of Naval Research (ONR) Multidisciplinary University Research Initiative (MURI) under Grant No. N00014-20-1-2325. A.C. acknowledges support from the Center for Integrated Nanotechnologies, an Office of Science User Facility operated for the U.S. Department of Energy (DOE) Office of Science, and the Laboratory Directed Research and Development program at Sandia National Laboratories. Sandia National Laboratories is a multimission laboratory

managed and operated by National Technology & Engineering Solutions of Sandia, LLC, a wholly owned subsidiary of Honeywell International, Inc., for the U.S. DOE's National Nuclear Security Administration under contract DE-NA-0003525. The views expressed in the article do not necessarily represent the views of the U.S. DOE or the United States Government.

Open access funding enabled and organized by Projekt DEAL.

Conflict of Interest

The authors declare no conflict of interest.

Data Availability Statement

The data that support the findings of this study are available from the corresponding author upon reasonable request.

Keywords

direct laser writing, photonic crystals, topological photonics, Weyl points

Received: August 12, 2021

Revised: November 2, 2021

Published online: December 10, 2021

- [1] S.-Y. Xu, I. Belopolski, N. Alidoust, M. Neupane, G. Bian, C. Zhang, R. Sankar, G. Chang, Z. Yuan, C.-C. Lee, S.-M. Huang, H. Zheng, J. Ma, D. S. Sanchez, B. Wang, A. Bansil, F. Chou, P. P. Shibayev, H. Lin, S. Jia, M. Z. Hasan, *Science* **2015**, 349, 613.
- [2] B. Q. Lv, H. M. Weng, B. B. Fu, X. P. Wang, H. Miao, J. Ma, P. Richard, X. C. Huang, L. X. Zhao, G. F. Chen, Z. Fang, X. Dai, T. Qian, H. Ding, *Phys. Rev. X* **2015**, 5, 031013.
- [3] B. Q. Lv, N. Xu, H. M. Weng, J. Z. Ma, P. Richard, X. C. Huang, L. X. Zhao, G. F. Chen, C. E. Matt, F. Bisti, V. N. Strocov, J. Mesot, Z. Fang, X. Dai, T. Qian, M. Shi, H. Ding, *Nature Physics* **2015**, 11, 724.
- [4] F. Arnold, M. Naumann, S.-C. Wu, Y. Sun, M. Schmidt, H. Borrmann, C. Felser, B. Yan, E. Hassinger, *Phys. Rev. Lett.* **2016**, 117, 146401.
- [5] N. P. Armitage, E. J. Mele, A. Vishwanath, *Rev. Mod. Phys.* **2018**, 90, 015001.
- [6] W. Meng, X. Zhang, T. He, L. Jin, X. Dai, Y. Liu, G. Liu, *J. Adv. Res.* **2020**, 24, 523.
- [7] B. Yan, C. Felser, *Ann. Rev. Condens. Matter Phys.* **2017**, 8, 337.
- [8] L. Lu, L. Fu, J. D. Joannopoulos, M. Soljačić, *Nat. Photonics* **2013**, 7, 294.
- [9] L. Lu, Z. Wang, D. Ye, L. Ran, L. Fu, J. D. Joannopoulos, M. Soljačić, *Science* **2015**, 349, 622.
- [10] B. Yang, Q. Guo, B. Tremain, R. Liu, L. E. Barr, Q. Yan, W. Gao, H. Liu, Y. Xiang, J. Chen, C. Fang, A. Hibbins, L. Lu, S. Zhang, *Science* **2018**, 359, 1013.
- [11] J. Noh, S. Huang, D. Leykam, Y. D. Chong, K. P. Chen, M. C. Rechtsman, *Nat. Phys.* **2017**, 13, 611.
- [12] M.-L. Chang, M. Xiao, W.-J. Chen, C. T. Chan, *Phys. Rev. B* **2017**, 95, 125136.
- [13] E. Goi, Z. Yue, B. P. Cumming, M. Gu, *Laser Photonics Rev.* **2018**, 12, 1700271.
- [14] S. Takahashi, S. Oono, S. Iwamoto, Y. Hatsugai, Y. Arakawa, *J. Phys. Soc. Jpn.* **2018**, 87, 123401.
- [15] A. Cerjan, S. Huang, M. Wang, K. P. Chen, Y. Chong, M. C. Rechtsman, *Nat. Photonics* **2019**, 13, 623.
- [16] S. Vaidya, J. Noh, A. Cerjan, C. Jörg, G. von Freymann, M. C. Rechtsman, *Phys. Rev. Lett.* **2020**, 125, 253902.
- [17] Z.-Y. Wang, X.-C. Cheng, B.-Z. Wang, J.-Y. Zhang, Y.-H. Lu, C.-R. Yi, S. Niu, Y. Deng, X.-J. Liu, S. Chen, J.-W. Pan, *Science* **2021**, 372, 271.
- [18] C. Devescovi, M. Garca-Dez, I. Robredo, M. B. de Paz, B. Bradlyn, J. L. Maes, M. G. Vergniory, A. Garca-Etxarri arXiv:2105.12725 2021.
- [19] Z. Yang, B. Zhang, *Phys. Rev. Lett.* **2016**, 117, 224301.
- [20] G. Ma, M. Xiao, C. T. Chan, *Nat. Rev. Phys.* **2019**, 1, 281.
- [21] W. Deng, X. Huang, J. Lu, F. Li, J. Ma, S. Chen, Z. Liu, *Sci. China Phys. Mech. Astronom.* **2020**, 63, 287032.
- [22] L. Luo, H.-X. Wang, Z.-K. Lin, B. Jiang, Y. Wu, F. Li, J.-H. Jiang, *Nat. Mater.* **2021**, 20, 794.
- [23] X.-Y. Mai, D.-W. Zhang, Z. Li, S.-L. Zhu, *Phys. Rev. A* **2017**, 95, 6.
- [24] T. Dubček, C. J. Kennedy, L. Lu, W. Ketterle, M. Soljačić, H. Buljan, *Phys. Rev. Lett.* **2015**, 225301.
- [25] R. Li, B. Lv, H. Tao, J. Shi, Y. Chong, B. Zhang, H. Chen, *Natl. Sci. Rev.* **2020**, 8, nwa192.
- [26] Q. Lin, M. Xiao, L. Yuan, S. Fan, *Nat. Commun.* **2016**, 7, 13731.
- [27] Y. Zhang, Y. Zhu, *Phys. Rev. A* **2017**, 96, 013811.
- [28] S.-L. Chua, L. Lu, J. Bravo-Abad, J. D. Joannopoulos, M. Soljačić, *Opt. Lett.* **2014**, 39, 2072.
- [29] I. n. García-Elcano, A. González-Tudela, J. Bravo-Abad, *Phys. Rev. Lett.* **2020**, 125, 163602.
- [30] L. Ying, M. Zhou, M. Mattei, B. Liu, P. Campagnola, R. H. Goldsmith, Z. Yu, *Phys. Rev. Lett.* **2019**, 123, 173901.
- [31] C. Fang, M. J. Gilbert, X. Dai, B. A. Bernevig, *Phys. Rev. Lett.* **2012**, 108, 266802.
- [32] M. M. Hirschmann, A. Leonhardt, B. Kilic, D. H. Fabini, A. P. Schnyder, *Phys. Rev. Mater.* **2021**, 5, 054202.
- [33] T.-G. Chen, J.-R. Jiao, H.-Q. Dai, D.-J. Yu, *Phys. Rev. B* **2018**, 98, 214110.
- [34] B. Roy, P. Goswami, V. Juričić, *Phys. Rev. B* **2017**, 95, 201102.
- [35] F. Li, X. Huang, J. Lu, J. Ma, Z. Liu, *Nat. Phys.* **2018**, 14, 30.
- [36] M. Deubel, G. von Freymann, M. Wegener, *Nat. Mater.* **2004**, 3, 444.
- [37] S. G. Johnson, J. D. Joannopoulos, *Opt. Express* **2001**, 8, 173.
- [38] R. Resta, *J. Phys.: Condens. Matter* **2000**, 12, R107.
- [39] V. Liu, S. Fan, *Comp. Phys. Commun.* **2012**, 183, 2233.
- [40] T.-H. Kao, L.-Y. C. Chien, Y.-C. Hung, *Opt. Express* **2015**, 23, 24416.
- [41] I. Karakasoglu, M. Xiao, S. Fan, *Opt. Express* **2018**, 26, 21664.
- [42] M. Saba, M. Thiel, M. D. Turner, S. T. Hyde, M. Gu, K. Grosse-Brauckmann, D. N. Neshev, K. Mecke, G. E. Schröder-Turk, *Phys. Rev. Lett.* **2011**, 106, 103902.
- [43] S. Takahashi, T. Tajiri, Y. Ota, J. Tatebayashi, S. Iwamoto, Y. Arakawa, *Appl. Phys. Lett.* **2014**, 105, 051107.
- [44] J. S. Oakdale, J. Ye, W. L. Smith, J. Biener, *Opt. Express* **2016**, 24, 27077.
- [45] A. Cerjan, C. Jrg, S. Vaidya, S. Augustine, W. A. Benalcazar, C. W. Hsu, G. von Freymann, M. C. Rechtsman, arXiv:2104.09603 2021.
- [46] D. B. Fullager, G. D. Boreman, T. Hofmann, *Opt. Mater. Express* **2017**, 7, 888.